A Novel MAMP Antenna Array Configuration for Efficient Beamforming

Dimitra D. Kalyva(✉), Dimitrios K. Ntaikos, and Constantinos B. Papadias

Athens Information Technology, 44 Kifissias Ave., 15125 Athens, Greece
{dkal,dint,cpap}@ait.gr

Abstract. Multi-Active Multi-Passive (MAMP) antenna arrays with reduced number of active elements are studied, for matching the patterns of all-active uniform linear arrays. Based on previous work on MAMP antenna arrays, we present a novel configuration, namely a circular one. By jointly calculating the PEs' loads and baseband weights of the proposed MAMP array, we can produce a radiation pattern similar to that of a ULA with accuracy up to 97.5%, while the number of AEs is reduced by 33% and in some cases with suppressed side lobes. Moreover, a reduction in the width of the array by 3 times is achieved. Thus, the complexity, compactness and cost of the antenna array can be reduced without compromising the quality of the resulting beam.

Keywords: Multi-active multi-passive (MAMP) arrays · Hybrid antenna arrays · Load and weight optimization

1 Introduction

Multi-active multi-passive (MAMP) antenna arrays are RF devices that consist of a small number of active elements (AE) where each AE is surrounded by multiple passive elements (PEs). The PEs are connected to variable loads, usually capacitors. Adjusting these load values leads to changes in the far field radiation pattern of the MAMP antenna. This enables the implementation of adaptive control techniques on the antenna. To this end, a MAMP antenna system of n active elements can shape a directive beam in such a way that it matches the beam of a conventional m-element uniform linear array (ULA), where $m > n$. The efficiency of this methodology is identified not only in the gain of the transmission, but also in the number of RF chains used, which is considerably smaller. In this paper, we are investigating a circular MAMP (C-MAMP) layout. The logic behind the creation of the C-MAMP antenna array lies in the theory of parasitic antennas [1].

While the single-active multi-passive (SAMP) antenna arrays, consisting of a single AE and multiple PEs, have been thoroughly studied, little has been said about the MAMP antenna arrays. This paper is based on and is an extention of the study presented in [2]. While in classical all-active arrays beamforming involves baseband signal processing, so that the gain is maximized or minimized

V. Poulkov (Ed.): FABULOUS 2019, LNICST 283, pp. 297–305, 2019.
https://doi.org/10.1007/978-3-030-23976-3_26

depending on the desired directions, in parasitic antenna arrays beamforming is achieved through the control of the loads of the passive elements. This adaptive control is implemented via the *Alternating Optimization Stochastic Beamforming Algorithm* (AO-SBA), which is rigorously explained in [2].

This work is organized as follows: in Sect. 2 we present the considered MAMP architecture; a short summary and the state-of-the-art methods are presented in Sect. 3; Sect. 4 is devoted to the presentation of our simulation results; finally, Sect. 5 summarizes the findings.

2 MAMP Antenna Arrays

In this paper we introduce a new circular topology of the MAMP antenna array, which differs from the previously studied rectangular MAMP (R-MAMP), in the way the parasitic elements are placed. More specifically, while the AEs remain parallel to the z-axis, with their centers lying on the x-axis at a distance $l_a = \lambda/2$ from one another, the PEs are positioned in such a way that each cluster forms a circle around its corresponding AE, of radius $l_p = 0.22\lambda$, lying in the x-y plane, as it is presented in the following Fig. 1. Hence, should the position of an AE be: $(x_a, 0)$, then the corresponding positions of the N_p PEs of its cluster would be given by the expression:

$$x_{pi}\big(i = 1 : N_p\big) = x_a + l_{pi} \cdot cos(\theta_i)$$
$$y_{pi}\big(i = 1 : N_p\big) = l_{pi} \cdot sin(\theta_i)$$

where θ_i denotes the angle between the $x - axis$ and the line segment with edges $(x_a, 0)$ and (x_{pi}, y_{pi}).

It is noted that since the PEs are placed symmetrically around the AE, angle θ_i will vary depending on the number of PEs selected each time.
We denote:

$$N_a : \text{the number of AEs}$$
$$N_p : \text{the number of PEs (constituting each AE cluster)}$$

And so it will be:

$$\theta_i\big(i = 1 : N_p\big) = \frac{360}{N_p} \cdot (i - 1)$$

However, the topology described in this paper, is vulnerable to present overlaps between the PEs of neighboring clusters belonging to neighboring AEs. In order to avoid such phenomena, the two distances l_a and l_p must satisfy the following condition:

$$l_a > 2 \cdot l_p$$

As far as the antenna elements are concerned, they are considered to be linear and ideal cylindrical dipoles of length $l = \lambda/2$ and of radius $r = \lambda/100$.

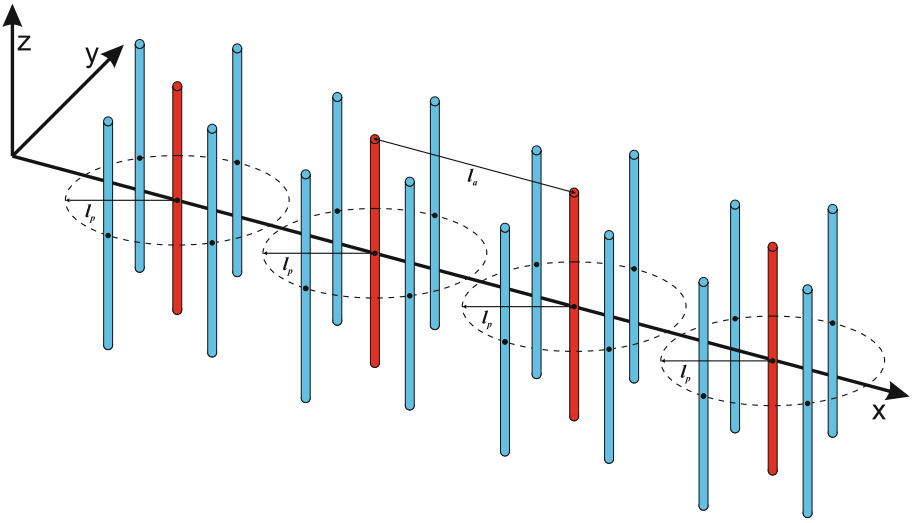

Fig. 1. Layout of the proposed C-MAMP antenna array with 4AEs (red dipoles) and 4PEs (blue dipoles) per AE. (Color figure online)

In order to compute the impedance matrix Z, all mutual effects that appear among all the side-by-side dipoles are taken into account, regardless of the fact that the inter-element distance might be large enough for it to be omitted.

The radiation intensity of the antenna, α, the complex normalized current vector on the antenna elements, i, and the voltage vector, v, are described through the expressions:

$$\alpha(\phi) = i^T \cdot s(\phi)$$
$$i(X, v) = (Z + X)^{-1} \cdot v$$

where: $s(\phi)$ is the respective steering vector at a given azimuth angle ϕ_0, X is the load reactance matrix that adjusts the radiation pattern of the antenna array and Z is the matrix representing the mutual impedance between each and every pair of the antenna elements.

The analytical expressions of the matrices X and Z for our case, where $N_a = 4$ and $N_p = 6$, are then given as:

$$X_i = \begin{vmatrix} x_i(1) & 0 & 0 & 0 & 0 & 0 & 0 \\ 0 & x_i(2) & 0 & 0 & 0 & 0 & 0 \\ 0 & 0 & x_i(3) & 0 & 0 & 0 & 0 \\ 0 & 0 & 0 & R_a & 0 & 0 & 0 \\ 0 & 0 & 0 & 0 & x_i(4) & 0 & 0 \\ 0 & 0 & 0 & 0 & 0 & x_i(5) & 0 \\ 0 & 0 & 0 & 0 & 0 & 0 & x_i(6) \end{vmatrix}$$

$$X = \begin{vmatrix} X_1 & 0_{7\times7} & 0_{7\times7} & 0_{7\times7} \\ 0_{7\times7} & X_2 & 0_{7\times7} & 0_{7\times7} \\ 0_{7\times7} & 0_{7\times7} & X_3 & 0_{7\times7} \\ 0_{7\times7} & 0_{7\times7} & 0_{7\times7} & X_4 \end{vmatrix}$$

$$Z = [z_{ij}] \quad : (i, j) \in \{(1...28), (1...28)\}$$

3 State-of-the-art

Although quite a few studies have been carried concerning the single-RF ESPAR antennas, [3], little has been done when it comes to MAMPs, and therefore the bibliography on this subject is very limited.

Researchers working on the topic have presented their work in [4], where they show the cross-correlation coefficient between an estimated beam pattern and a desired one, to optimize a function that calculates the loads of a SAMP antenna. The minimization task was approached by using a steep gradient scheme based on a simultaneous perturbation stochastic approximation (SPSA) method [5]. The gradient was approximated by using the two-sided finite-difference method [6]. Additionly, in [4], the authors have incorporated a smoothing technique, which provides better convergence properties [7]. However, since only a single AE antenna was considered, the steering of the beam was mainly enabled due to the circular geometry of the proposed antenna. Thus, beam steering could not have been achieved solely by the tuning of the loads, supposing that a linear geometry had been selected. Their algorithm is known as the Stochastic Beamforming Algorithm (SBA).

One rather straightforward solution for optimizing the radiation pattern of a MAMP antenna array and enabling the rotation of the beam, is to directly extend the SBA for SAMP antennas in [4] to the MAMP arrays. In our case though, a different initialization of the non-zero voltage (weight) values proved essential. Instead of choosing unitary initial values, *the considered complex weights are given by the steering vector of the corresponding ULA* (ULA with AEs equal to those of the MAMP) at a certain direction of arrival ϕ_0.

As we will present in the numerical evaluation section, the estimation performance of this approach proved to be quite limited. After extensive experimentation, we used the following extensions of the SBA for the MAMP antenna arrays, depending on the selection of its smoothing sequence $(\beta_m)_{m=1}^{M}$:

- SBA-SS1: Stochastic Beamforming Algorithm with the *smoothing sequence 1*, as the one used in [4], i.e., $\{40, 35, 30, 20, 10, 2.8, 2.4, 2, 1.5, 1, 0.75, 0.4, 0.2, 0.1\}$.
- SBA-SS2: Stochastic Beamforming Algorithm with the *smoothing sequence 2*, $\beta_m = \beta_{m-1}/2,\ \beta_0 = 5,\ m = 1, \ldots, 13$. This selected sequence has optimal decaying, as reported in [8].

4 Numerical Evaluation

For our numerical investigation we examine the effect of the PEs on multiple active ones. More precisely, we attempt to match the radiation pattern of a 6-element ULA with the resulting beam of a C-MAMP array consisting of 4 AEs and 6 PEs. To that extend, an improvement of the radiation pattern of a 4-ULA is achieved, without adding any further active elements, but only passive ones.

As mentioned above, the algorithm presented in [2] has been used, so as to compute the optimization loads and weights (voltage vector). The parameters set in the algorithm are: $\tau = 100$, $N_m = 10.000$, $T_{er} = 10^{-6}$, $eps = 10^{-10}$, $\beta_m = \frac{\beta_{m-1}}{3}$, $\beta_0 = 3$, $m = 1, ..., 25$.

The initial topology under examination is the C-MAMP with 4 AEs and 4 PEs at an azimuth angle of $\phi_0 = 90°$, which is compared to the 4-ULA and 6-ULA. In order to validate the improvement of the resulting beam as the number of PEs increases, we also use 6 PEs, while maintaining the azimuth angle and the number of AEs. The resulting figures confirm our initial assumptions, and an improvement is observed. More specifically, not only does the steady state error decrease, but also the convergence towards it is smoother. The latter is due to the fact that, by increasing the number of parasitic elements the algorithm converges to its stable state more quickly, and therefore, the resulting curve becomes smoother for the same number of iterations m. According to Fig. 2(a) and (b), we see that the C-MAMP antenna matches quite well the pattern of the 6-ULA in both cases (the mismatch error is around 6.83% and 3.23%, respectively). In Figs. 3(a) and (b), where we present the azimuthal plane of the radiation pattern, it is obvious that the C-MAMP matches accurately the pattern of the 6-ULA.

Next, we evaluate the flexibility of our proposed C-MAMP antenna array configuration in terms of its ability to rotate the radiation pattern towards any direction, and thus we change the azimuth angle to $\phi_0 = 60°$, while the topology still has 4 PEs per AE. As depicted in Fig. 4(a), the C-MAMP array does converge to the pattern of the 6-ULA, with a matching error of around 5.86%. In order to reduce the matching error, we increase the number of the PEs to 6, and observe that it improves (in Fig. 4(b) the matching error is around 5.58%). As explained in the previous case, similarly here, apart from the error reduction, we observe more smoothness in its convergence. However, the smoothness is noted only for $m > 10$, whereas for $5 < m < 10$ there is a steep increase of the error. This may be caused by insufficient number of iterations N_m of the algorithm at that point, or by the need of a slightly different parameter, among those used in the adaptive algorithm. In any case, this doesn't affect the final result significantly, since the steady state error convergence is as expected. In Figs. 5(a) and (b) we notice the matching of the radiation patterns.

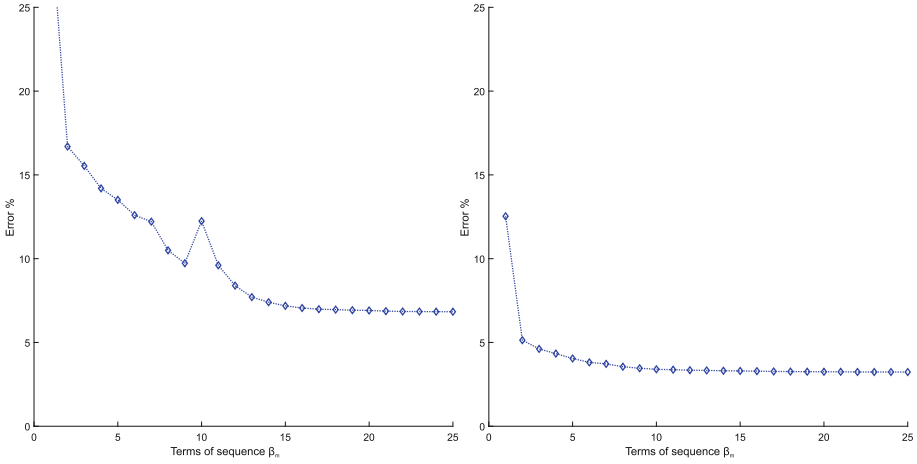

(a) (b)

Fig. 2. Matching error at $\phi_0 = 90°$ between a 6-ULA and the C-MAMP with: (a) 4AEs and 4PEs and, (b) 4AEs and 6PEs.

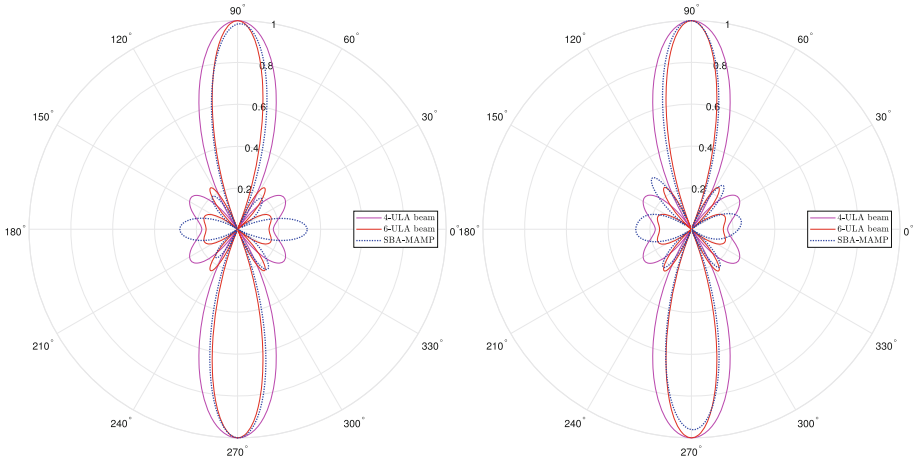

(a) (b)

Fig. 3. Radiation pattern comparison at $\phi_0 = 90°$ between 4-ULA, 6-ULA and C-MAMP with: (a) 4AEs and 4PEs and, (b) 4AEs and 6PEs.

As a final confirmation step, we set the azimuth angle to $\phi_0 = 45°$, maintaining the number of PEs at 4. Figure 6(a) confirms the adaptability of the C-MAMP antenna array, since the resulting matching error is around 3.52%. In addition to that, in Fig. 7(a) we observe a narrower beam with a significant reduction in the side lobes. Finally, the case of $\phi_0 = 70°$ azimuth angle is considered, although, this time the number of PEs used is set to 8. Once again, the

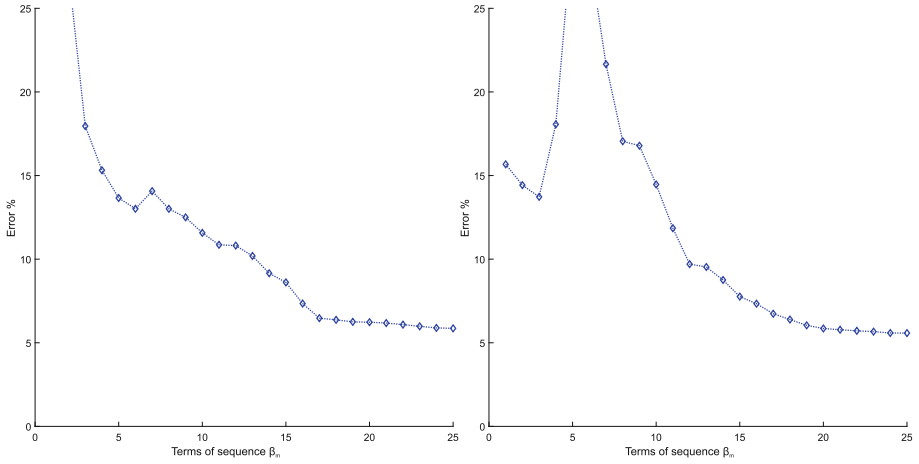

Fig. 4. Matching error at $\phi_0 = 60^\circ$ between a 6-ULA and a MAMP antenna array with: (a) 4AEs and 4PEs and, (b) 4AEs and 6PEs.

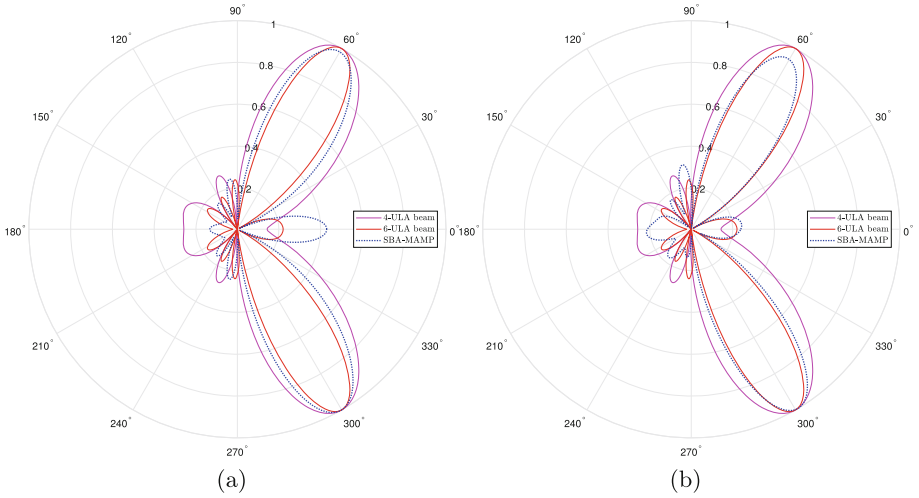

Fig. 5. Radiation pattern comparison at $\phi = 60^\circ$ between a 4-ULA, a 6-ULA and a MAMP antenna array with: (a) 4AEs and 4PEs and, (b) 4AEs and 6PEs.

matching error in Fig. 6(b) is around 2.49% and the produced beam in Fig. 7(b) matches to a great extend, the radiation pattern of the 6-ULA. In both cases, the figures referring to the steady state errors reconfirm our above mentioned comments concerning their convergence.

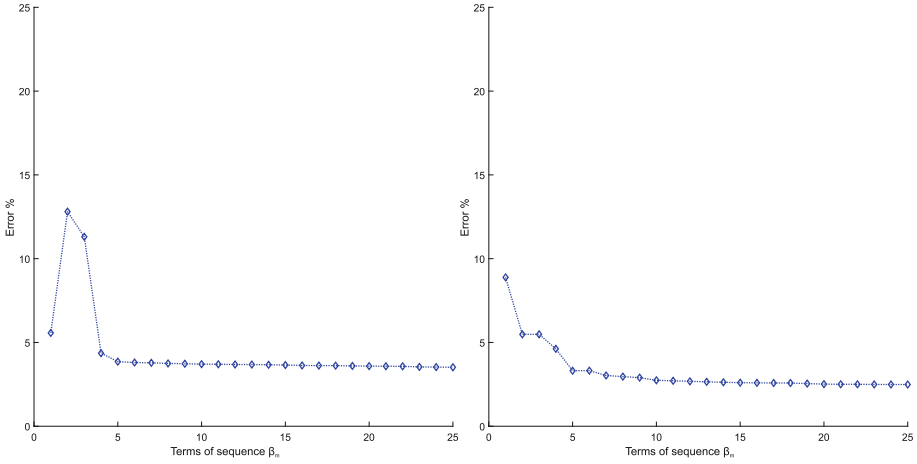

Fig. 6. Matching error between a 6-ULA and a MAMP antenna array with: (a) 4AEs and 4PEs at 45° and, (b) 4AEs and 8PEs at 70°.

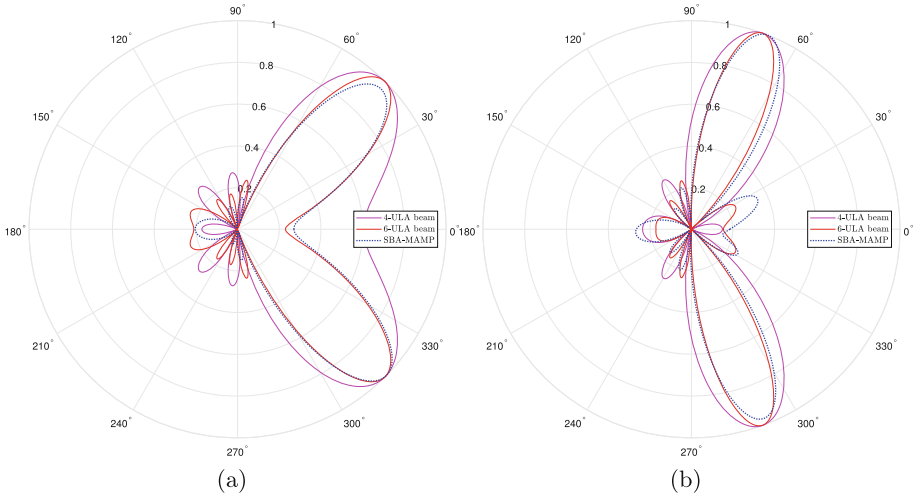

Fig. 7. Radiation pattern comparison between 4-ULA, 6-ULA and MAMP antenna array with: (a) 4AEs and 4PEs at 45° and, (b) 4AEs and 8PEs at 70°.

5 Conclusions

In this paper, an altered version of the R-MAMP antenna array with a circular topology of the passive elements was proposed. The so-called C-MAMP antenna array provides greater compactness compared to the R-MAMP topology (0.44λ compared to 1.2λ on the y-direction), which can be very useful when referring

to large structures. Both the efficiency of the topology according to the number of passive elements used, and its versatility relative to pattern rotation, were examined. As evidenced by the numerical simulations, the C-MAMP can successfully replicate the radiation pattern of the 6-ULA, in various azimuth angles, by reducing the number of AEs from 6 to 4. This corresponds to a 33% reduction of the RF chains needed to create the same beam pattern, thus reducing the overall cost of operating such a MAMP antenna array. Finally, an increase in the number of the passive elements has been shown to provide greater accuracy in the results. Future expansions of the problem include the development of an actual C-MAMP antenna system, in order to compare the simulated results with measured ones. This will verify the correctness of the proposed model, as well as its efficiency in real-life problems.

References

1. Kalis, A., Kanatas, A.G., Papadias, C.B.: Parasitic Antenna Arrays for Wireless MIMO Systems. Springer, New York (2014). https://doi.org/10.1007/978-1-4614-7999-4
2. Papageorgiou, G.K., Ntaikos, D.K., Papadias, C.B.: Efficient beamforming with multi-active multi-passive antenna arrays. In: 2018 IEEE 19th International Workshop on Signal Processing Advances in Wireless Communications (SPAWC), pp. 1–5, June 2018. https://doi.org/10.1109/SPAWC.2018.8445890
3. Marantis, L., et al.: The pattern selection capability of a printed ESPAR antenna. In: 2017 11th European Conference on Antennas and Propagation (EUCAP), pp. 922–926, March 2017. https://doi.org/10.23919/EuCAP.2017.7928841
4. Barousis, V., et al.: A stochastic beamforming algorithm for ESPAR antennas. IEEE Antennas Wirel. Propag. Lett. **7**, 745–748 (2008)
5. Spall, J.C.: Introduction to Stochastic Search and Optimization: Estimation, Simulation, and Control, vol. 65. Wiley, New York (2005)
6. Wilmott, P., Howison, S., Dewynne, J.: The Mathematics of Financial Derivatives: a Student Introduction. Cambridge University Press, Cambridge (1995)
7. Styblinski, M., Tang, T.S.: Experiments in nonconvex optimization: stochastic approximation with function smoothing and simulated annealing. Neural Netw. **3**(4), 467–483 (1990)
8. Chin, D.C.: A more efficient global optimization algorithm based on Styblinski and Tang. Neural Netw. **7**(3), 573–574 (1994)